Computational and Functional Evaluation of a Microfluidic Blood Flow Device

Richard J. Gilbert,*† Hyesung Park,* Marco Rasponi,‡ Alberto Redaelli,‡ Barry Gellman,† Kurt A. Dasse,† and Todd Thorsen*

The development of microfluidic devices supporting physiological blood flow has the potential to yield biomedical technologies emulating human organ function. However, advances in this area have been constrained by the fact that artificial microchannels constructed for such devices need to achieve maximum chemical diffusion as well as hemocompatibility. To address this issue, we designed an elastomeric microfluidic flow device composed of poly (dimethylsiloxane) to emulate the geometry and flow properties of the pulmonary microcirculation. Our chip design is characterized by high aspect ratio (width > height) channels in an orthogonally interconnected configuration. Finite element simulations of blood flow through the network design chip demonstrated that the apparent pressure drop varied in a linear manner with flow rate. For simulated flow rates <250 μl min^{-1}, the simulated pressure drop was <2000 Pa, the flow was laminar, and hemolysis was minimal. Hemolysis rate, assayed in terms of [total plasma hemoglobin (TPH) (sample − control)/(TPH control)] during 6 and 12 hour perfusions at 250 μl/min, was <5.0% through the entire period of device perfusion. There was no evidence of microscopic thrombus at any channel segment or junction under these perfusion conditions. We conclude that a microfluidic blood flow device possessing asymmetric and interconnected microchannels exhibits uniform flow properties and preliminary hemocompatibility. Such technology should foster the development of miniature oxygenators and similar biomedical devices requiring both a microscale reaction volume and physiological blood flow. *ASAIO Journal* 2007; 53:447–455.

Microfluidic devices, consisting of a network of channels with diameters comparable to human arterioles (~90 μm), are ideal platforms for the study of the transport dynamics and biochemistry of biologic fluids. Over the past 15 years, such devices have been broadly applied in the fields of analytical chemistry,[1–5] tissue engineering,[6–9] and biomimetic devices.[10–12] Due to the explicit geometry and fluid driving pressures used in these microdevices, the Reynolds number (Re) for the operating fluid is usually much less than 100, leading to characteristically laminar conditions. The development of microfluidic devices designed to emulate physiologic flow systems, such as the capillary microcirculation, has particularly stringent design requirements due to the need to maintain the viability of rather fragile red and white blood cells. Such microchannels need to incorporate a relatively small diffusive boundary layer to allow chemical efficiency while maintaining broad enough dimensions to minimize adverse flow conditions. This design rule is evident, for example, in the case of artificial lung technologies designed to deliver oxygen to red blood cells either via oxygen transport across hollow fiber membranes,[13,14] or following oxygen generation by photolysis.[15,16] Such systems require short diffusion distances in order to achieve rapid oxyhemoglobin formation yet sufficiently large hydraulic capillary diameters to minimize shear stress and flow irregularities. In this report, we describe the design, fabrication, and functional validation of an elastomeric microfluidic network, consisting of gas-permeable poly (dimethyl-siloxane) (PDMS) that closely emulates the geometry of pulmonary microcirculation beds.

Methods

Basic Design Elements for a Microfluidic Capillary Network

Microfluidic blood flow devices are generally limited by large pressure drops and complex channel geometries, conditions that may be associated with impaired hemocompatibility. Scaling up of these networks to accommodate physiologically relevant blood flow rates (l/min) is very challenging. We have previously examined in detail the relationships between microchannel geometry and configuration, flow and oxygen diffusion in a microcapillary device.[17,18] Acknowledging the presence of relatively large viscous forces in most microfluidic devices, and the resulting effect on shear stress,[19,20] it has been previously suggested that blood flow microchannels embodying a branching network require a minimum diameter of 100 μm.[21] Although this channel diameter is considerably larger than native pulmonary capillaries (~10 μm), this diameter is analogous to that of the branching pulmonary arterial system[22–25] and thus may constitute a reasonable design template. Such a design represents a pragmatic compromise as it may itself introduce regions of flow instability not present in native pulmonary capillaries. The mass transfer properties of an array of microchannels with hydraulic diameters on the order of 100 μm was previously characterized analytically through a simple convective mass transfer model accounting for the diffusivity of oxygen in aqueous solution,[17] and

*Department of Mechanical Engineering, Massachusetts Institute of Technology, Cambridge, Massachusetts, U.S.A.; †Levitronix Medical, Waltham, Massachusetts, U.S.A.; ‡Department of Bioengineering, Politecnico di Milano, Milan, Italy.

Submitted for consideration August 2006; accepted for publication in revised form March 2007.

Reprint Requests: Todd Thorsen PhD, Department of Mechanical Engineering, Massachusetts Institute of Technology, 77 Massachusetts Avenue, 3-248, Cambridge, MA 02135, U.S.A.

DOI: 10.1097/MAT.0b013e3180a5e8ab

deriving the Peclet number as a measure of the ratio of the convective to diffusive mass transport both analytically and experimentally. However, preliminary hemocompatibility experiments to assay thrombogenesis by microscopic visualization for devices possessing a 100 μm $\times$ 100 μm channel diameters and a 90-degree branching configuration during flow (0.1–0.64 ml/min) of anticoagulated blood (ACT >300 seconds) revealed thrombus at 25% of channel inlets/outlets and bifurcations as early as 20 minutes.[26] As a result, we considered an open network of diamond-shaped posts with the goal of minimizing reduced flow regions and thus reducing the rate of thrombus.

As a basic, scalable building block to minimize damaging tangential shear forces, we adopted an asymmetrically configured microchannel network design (**Figure 1**). Our design was similar to the computational model of the human pulmonary capillary system described by Huang *et al.*[27] and the network model of endothelialized microcapillaries proposed by Shin *et al.*[28] The latter device embodied a microcapillary system with variable channel widths (ranging from 35 μm to 5 mm) and uniform channel depth (35 μm) and was designed to specifically emulate microvascular physiology and promote the viability of attached cells. Similarly, Kaazempur-Mofrad *et al.* proposed a variation on this design for the purpose of renal filtration,[29] based on prior fractal-based design concepts.[30] Our microfluidic chip design incorporated the following specific physical properties. First, the individual channels possess a high aspect ratio, exhibiting a width of 1.197 mm and a channel height of 0.1 mm. The width of the inlet and outlet channels is 3.38 mm, while the overall footprint of the microfluidic array is 2 $\times$ 2 cm. The channel height was derived directly from prior computational and experimental results.[17] The channel width was chosen empirically on the basis of practical limitations of current microfabrication capabilities, and was not systematically varied in the current study. Second, the set of microchannels comprising the two-dimensional aligned chip are each interconnected with four other channels in a network configuration, thus allowing alternative flow pathways in the event of single channel occlusion while minimizing the establishment of detrimental pressure gradients that would be observed using a right-angle hierarchically branching channel architecture.

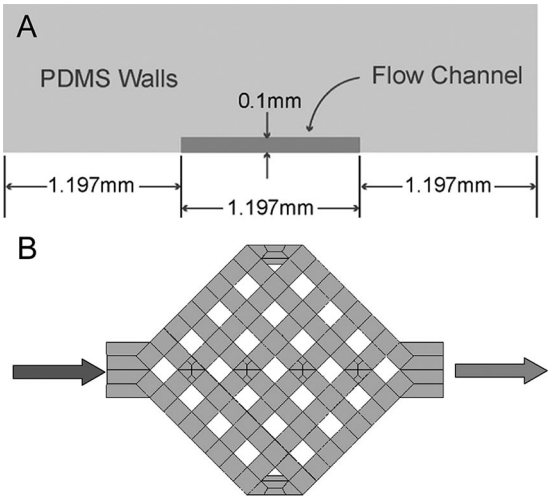

Figure 1. Microfluidic device using a network construct. A novel construct was used that combined low channel height for efficient diffusion with relatively broad channel width to minimize shear stress. Shown here are diagrammatic representations of the microchannel network from the perspective of (**A**) an individual microchannel illustrating the asymmetric geometry (height of channel is relatively small compared with channel width). (**B**) Top-down view of the overall microchannel network depicting the set of orthogonal interconnections characteristic of the chip configuration.

Generation of a Finite Element Model to Simulate Flow Fields and Hemocompatibility

To simulate flow fields and hemocompatibility for the proposed microfluidic chip, a geometrical model was created and meshed through CFD-GEOM (CFDRC, Huntsville, AL). Simulations of blood flow were obtained for local velocity and Reynolds number at varying flow rates (ranging from 25 μl to 1 ml/min). The Reynolds number, defined as the ratio between inertial and viscous forces, may be represented as follows:

$$\mathrm{Re} = \frac{\rho U D}{\mu} \tag{1}$$

where ρ is the fluid density, U is the velocity, D is the characteristic length, and μ is the viscosity.

In the microfluidic realm, flow is generally laminar, with viscous forces dominating over inertial forces. To account for the non-Newtonian behavior of blood, viscosity was assumed to be variable and the power law model proposed by Ballyk was used.[31]

$$\mu = \lambda|\dot{\gamma}|^{n-1} \tag{2}$$

$$\lambda(\dot{\gamma}) = \mu_\infty + \Delta\mu \exp\left[-\left(1 + \left(\frac{|\dot{\gamma}|}{a}\right)\right)\exp\left(-\frac{b}{|\dot{\gamma}|}\right)\right] \tag{3}$$

$$n(\dot{\gamma}) = n_\infty + \Delta n \exp\left[-\left(1 + \left(\frac{|\dot{\gamma}|}{c}\right)\right)\exp\left(-\frac{d}{|\dot{\gamma}|}\right)\right] \tag{4}$$

where λ is the consistency parameter, $\dot{\gamma}$ is the local shear rate, μ_∞ is the limiting Newtonian viscosity, and a, b, c, d, $\Delta\mu$, and n_∞ are constant values.

To generalize the above to multidimensional flows, μ may be is replaced by the stress tensor, τ_{ij}, $\dot{\gamma}$ is replaced by the rate of strain tensor, $D_{ij} = \frac{1}{2}(\delta u_i/\delta x_j + \delta u_j/\delta x_i)$, and the magnitude of $\dot{\gamma}$ is replaced by the second invariant of the rate of strain tensor, D_{II}.[32] The momentum equation for the i^{th} component of the velocity vector, u, solved by the commercial code thus becomes:

$$\rho\frac{\partial(u_i)}{\partial t} + \nabla\cdot(\rho\vec{u}u_i) = \frac{\partial(-p + \tau_{ii})}{\partial x_i} + \frac{\partial\tau_{ji}}{\partial x_j} + \frac{\partial\tau_{ki}}{\partial x_k} \tag{5}$$

and the mass conservation equation becomes:

$$\nabla\cdot\vec{u} = 0 \tag{6}$$

assuming the fluid is incompressible. The density of the blood was set to 1.057 kg/m^3, calculated considering a hematocrit value of 0.45 through:

$$\rho_{blood} = \rho_{plasma}\cdot(1 - Ht) + \rho_{cells}\cdot Ht \tag{7}$$

with ρ_{plasma} = 1.030 kg/m^3, the density of the plasma, and ρ_{cells} = 1.090 kg/m^3, the density of platelets and blood cells.[33] No-slip boundary conditions were imposed on all solid surfaces, while for each numerical analysis a normal velocity to

the inlet channel of the model was applied so that the flow rate varied between $3{\cdot}10^{-1}$ μl/min to $6{\cdot}10^{2}$ μl/min in eight simulations. For each simulation, the convergence was guaranteed by decreasing the relative values of the residuals (for the three velocity components and the pressure) below the threshold of $1{\cdot}10^{-6}$. Moreover, the mass flow balance was computed and verified to be at least four orders of magnitude lower than the inlet mass flow rate.

The exposure of the red blood cells (RBC) to shear stress for varying periods of time causes determinable effects on the RBC cell membrane.[34] Hemolysis, expressed in terms of free hemoglobin, may be explicitly associated with shear stress and exposure time by the power law calculations of Blackshear.[35] Giersiepen, furthermore, proposed a power-law formulation to relate levels of turbulent shear stress with hemolysis.[36] The power-law model relating the concentration of free hemoglobin (Hb), the shear stress acting on the blood cell and time of exposure to the shear stress condition has the general form of:

$$\Delta Hb/Hb\% = C t^{a} \tau^{b} \tag{8}$$

where C, a, and b are constant values and depend on the species from which the blood was derived (*e.g.*, human, bovine). ΔHb represents the increase of free hemoglobin in the blood, which is strictly related to RBC damage. A blood damage index (BDI), analogous to the rate of hemolysis, may be computed and expressed as percentage of total hemoglobin for a set of RBCs moving in a generic pathline, adding the various sublytic (*i.e.*, elemental) contributions. A method to calculate the BDI, based on the above relationships, has been proposed by Zimmer *et al.*[37] and Lim *et al.*[38] The elemental contributions to hemolysis rate are given by the differential quotient of the following:

$$d(BDI) = a \cdot C \cdot t^{a-1} \cdot \tau(t)^{b}\, dt \tag{9}$$

which may also be written in discrete form as follows:

$$\Delta BDI = a \cdot C \cdot t_i^{a-1} \cdot \tau(t)_i^{b}\, \Delta t_i \tag{10}$$

where τ_i is the shear stress acting during the i^{th} observation interval Δt_i and t_i is the time it takes the blood cell to reach the i^{th} observation point, *i.e.*,

$$t_i = \sum_{f=1}^{i} \Delta t_f \tag{11}$$

The damage summation along a pathline can be calculated as the summation of the elemental contributions:

$$BDI = \int_{t_a}^{t} aC\Phi^{a-1}\, \tau(\Phi)^{b}\, d\Phi \tag{12}$$

whose discrete expression is:

$$BDI = \sum_{f=1}^{N} aCt_i^{a-1}\, \tau(t)_f^{b}\, \Delta t_f \tag{13}$$

where N is the total number of time intervals. The above hemolysis prediction model was implemented in CFD-ACE+ and hemolysis rates represented as a function of flow in the range of 125 to 1000 μl/min.

Fabrication of Microfluidic Capillary Network

The two-dimensional microchannel pattern was generated using AUTOCAD, after which the pattern was transferred to a transparency mask via a high resolution printer (3550 dpi). A master for replica molding was prepared from negative photoresist (SU-8, Microchem) on a 3-inch silicon wafer using standard photolithography. A microfluidic device was then fabricated from PDMS by replica molding from the previously constructed master using the technique of soft lithography.[39–41] PDMS (Sylgard 184, two-part elastomer) was chosen for as the device material due to its biocompatibility with blood, low cost, and ease of fabrication.[42] A 5:1 monomer/catalyst mixture was mixed, degassed, and poured on the SU-8 mold to an approximate 5 mm thickness. Subsequently, a 20:1 mixture of PDMS was prepared and poured onto a blank silicon wafer to a 5 mm thickness, constituting a substrate for the fluid channel. Both molds were again degassed under vacuum to remove air bubbles generated, while PDMS was poured onto the molds and baked at 80°C for 20 minutes. Once the PDMS was cured, the patterned structure was cut and peeled off from the master, which was previously treated with trichlorotrimethylsilane for seven minutes to minimize adhesion of the PDMS to the SU-8 mold. Holes for the inlets and outlets of the fluid channels were generated with a 20G Luer stub. This flow layer of PDMS was placed onto the substrate layer of PDMS and baked at 80°C for an additional three hours to form a covalent bond between the two layers. This assembly was then cut and peeled from the wafer, yielding the completed device.

Assessment of Hemocompatibility

Five sets of blood tests were performed to assay the rate of hemolysis and thrombosis generation in the microfluidic device. Bovine blood obtained from a slaughterhouse (Lemay, Goftstown, NH) with a normalized hematocrit of 29 to 30 was used (Autocrit Ultra 3) for each experiment. The age range of the blood was 24 to 120 hours. No difference was observed in regard to results as a function of age of the blood. Blood acquired from the slaughterhouse was treated as follows: A solution of 50,000 units heparin in 1 l sterile Dextrose (5%) was combined with approximately 4 gallons of blood obtained from an individual animal. The blood was then gently stirred to distribute the heparin into the fresh blood. The activated clotting time (ACT) was determined by conventional clinical methods and was found to be approximately 400 seconds at room temperature, an accepted value for during clinical cardiopulmonary bypass.[42–46] For assay of hemolysis, 10 ml samples of blood were collected from the device outlets at each time point (every 40 minutes for a total duration of 6 or 12 hours) and compared with a control blood sample that was flowed at the same rate but not through the microfluidic device. Both control and sample were collected and were centrifuged for 10 minutes at 3400 rpm to isolate the plasma. After centrifugation, 2 ml of the plasma was mixed with 1 ml cyanmethemoglobin, and the absorption rate was measured by a spectrophotometer (Thermo Spectronic) to calculate the total plasma hemoglobin

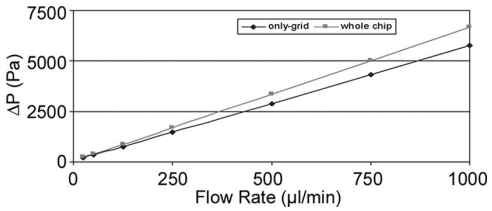

Figure 2. Relationship of pressure drop across the microfluidic chip to flow rate. A linear regression was computed in the case of the pressure drop over the entire chip, considering the grid alone, while excluding the entrance and exit ducts. Observe that the pressure drop increases linearly with flow rate. The two different lines represent the pressure drop of the central part (the grid with obstacles) and the entire chip (with entrance and exit ducts), in blue and red, respectively.

(TPH) (mg/dl) in terms of absorption × 242.65 + 3.07.[47] Hemolysis was represented as the [TPH (sample − control)/TPH (control)] during 6 and 12 hour infusions performed at room temperature, at a flow rate of 250 μl/min as predicted by prior simulation. Because the flow rate and sampling interval did not vary, further normalization procedures[48] were judged to be unwarranted. Thrombus formation was assessed by microscopic visualization of the channels with an upright light microscope (Industrial Products Group, Inc) at 5 and 10× magnification during and following flow through the microfluidic chip for 6 and 12 hours at 0.25 ml/min. Since early platelet activation events associated with activation are likely to be undetected by this method,[49,50] this assay should properly be regarded as a preliminary assessment of *in vivo* thrombogenesis.

Results

Model Results

The goal of the present modeling effort was to simulate the flow conditions existing within a model microfluidic chip and its impact on hemocompatibility of flowing blood. We specifically hypothesized that a microfluidic chip incorporating a decidedly asymmetric channel geometry (width ≫ height) and interacting microcapillaries would improve hemocompatibility while minimizing the diffusion distance from a hypothetical "active" surface. Because the pressure drop across such a device is considered a predictor of hemolysis risk, we modeled this property as an explicit function of the flow (10 μl–1 ml/min), considering flow through the grid alone and flow through the grid and inlet/outlet. A linear regression was computed for each of the two sets of data, using the following relationship, $\Delta p = \alpha V + p_o$, where the values of the constants α and p_o in the "grid-only case" are 5.7094 Pa·min/μl and 56.768 Pa, respectively. As shown in **Figure 2**, the modeled pressure drop varied in a linear manner with flow rate, with increased pressure drop evident for the whole chip vs. the grid alone for the higher range of flow rates (>500 μl/min). In the figure, two different linear regression curves were computed: the diamond symbols indicate the pressure drop across the central part of the device (the grid with the obstacles) while the square symbols indicate the pressure drop across the entire model (thus including the inlet and outlet channels). For relatively low flow rates (<250 μl/min), our simulations yielded a maximum value of pressure drop of about 2 kPa (about 15 mm Hg), conceptually similar to previous reports.[51] Accordingly, we used this flow as a reference value in subsequent simulations and functional testing. We provide in **Figure 3** the results of a finite element simulation of local velocity and viscosity in association with the above flow rate. The simulation predicted a fairly uniform velocity within the microfluidic construct with the exception of a few singular regions of high velocity near the inlet and outlet regions. Hemolysis was computed according to the Giersiepen model (**Figure 4**), which represented the relationship between the percent free hemoglobin in the blood and the imposed flow rate. The model predicted, for a flow rate of 250 μl/min, an associated hemolysis percentage of 6.89.

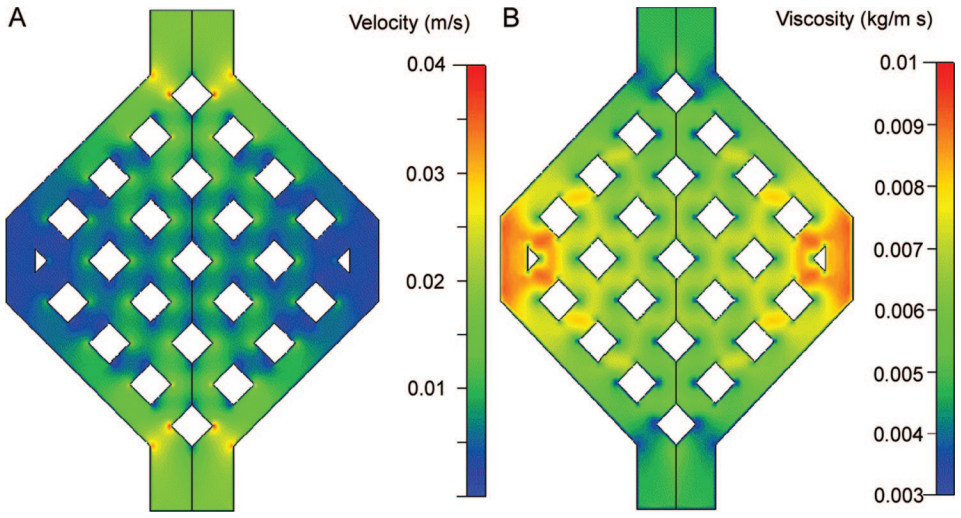

Figure 3. Computational simulation of local blood flow in microfluidic constructs. To determine local flow properties, and thus infer hemolysis risk, a geometrical model of the chip was created and meshed through CFD-GEOM software. Simulations were run at varying flow rates to ascertain both (**A**) local flow velocity and (**B**) local dynamic viscosity. Data were obtained at specific flow rate of 250 μl/min. The velocity images display a high degree of uniformity as a function of location in the chip. Local viscosity is directly correlated to the local shear rates and, consequently, to hemolysis risk.

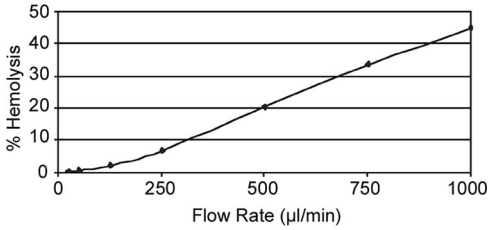

Figure 4. Computational simulation of the rate of hemolysis as a function of blood flow through microfluidic constructs. Hemolysis rates were simulated during flow through the microfluidic construct using a power law formulation (see Methods) and implemented in CFD-ACE+. Hemolysis rates are presented as a function of flow in the range of 125 μl to 1 ml/min.

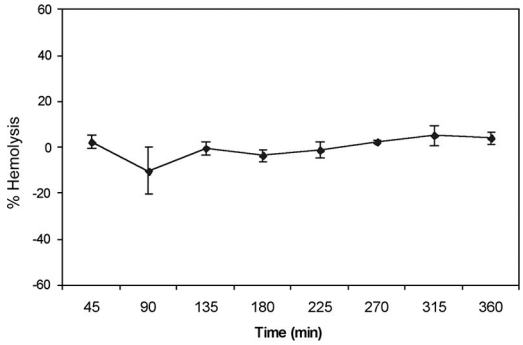

Figure 5. Determination of hemolysis during 6-hour perfusion through microfluidic device. Hemolysis was determined as a function of flow through the microfluidic construct (sample) compared with flow outside of the microfluidic construct (control) in four separate experiments Samples were obtained every 40 minutes over course of a 6-hour perfusion at a constant flow rate of 250 μl/min and total plasma hemoglobin derived by spectrophotometry. Hemolysis was represented as the TPH (sample − control)/TPH control for each time point and displayed as mean + SD. The hemolysis percentage was consistently <5.0% and did not increase significantly with the time of perfusion.

Although the overall non-Newtonian behavior of the blood was taken into account, our numerical model did not consider a well-known phenomenon occurring in small dimensional flow fields, the plasma skimming effect. Fahraeus and Lindquist noticed that, in small diameter tubes (<500 μm), the viscosity decreases because of the platelets, and the blood cells travel in the middle of the tube rather than close to its walls.[52] Even in the absence of a cylindrical geometry, this effect is conceivable, as Reinke *et al*. observed that, for a hematocrit of 0.45 and for tubes of about 100 μm diameter, the apparent viscosity is about 15 to 20% less than that measured at the macroscopic scale.[53] In our model, in which the smallest microchannels in the center of the device are 1197 μm (w) × 0.1 μm (h), the hydraulic diameter of the channel, defined by [4 A (area)/wetted perimeter], is ~180 μm; therefore, clearly the inclusion of additional terms to account for plasma skimming has the potential to improve the model. Moreover, the likelihood that we are overestimating the true viscosity implies that the results with respect to the pressure drop and hemolicity are "worse", rendering the model more conservative.

Experimental Hemocompatibility

Flow irregularities related to the geometry of the proposed microfluidic chip may result in enhanced shear stress conditions leading to increased hemolysis or significant variations of flow rate resulting in enhanced thrombogenesis. To address the former, the rate of hemolysis was obtained in 4 separate experiments and represented as the total plasma hemoglobin (TPH) (sample − control)/TPH (control) obtained over a 6 hour perfusion at a flow rate of 0.250 ml/min (**Figure 5**), a flow condition predicted by the above simulation to entail minimum hemolysis. Hemolysis rate assayed in this manner was <5.0% throughout the entire period of device perfusion. The microfluidic chips were further observed for possible thrombus deposition following these 6 hour perfusion experiments followed by a washout period. **Figure 6** represents a set of representative microfluidic chip images (n = 4 experiments). There was no visible evidence of thrombus deposition at any location in the chip. Additionally, in a single long-term (12 hour) experiment, we observed that the total plasma hemoglobin remained stable and not significantly different from the control for the entire infusion period (**Figure 7**), and there was no visible thrombus deposition.

Discussion

Microfluidic device development provides a basis for precise fluid mechanical and chemical control. However, the adaptation of such technology to blood flow devices introduces several risks, including high shear stress and flow instability, and thus may be associated with high rates of RBC fragility and hemolysis as well as platelet activation leading to thrombosis. Indeed, in an earlier generation of a two-dimensional microfluidic oxygenation device consisting of 100 μm^2 channels arborizing at right angles to each other, we observed a relatively high rate of hemolysis and significant thrombogenesis.[17,26] These results specifically implied the need to vary channel diameter and channel relationships at the points of channel bifurcation. Furthermore, in considering the channel shape necessary to achieve optimal convective mass transport of oxygen in a microfluidic channel,[17] the need for minimization of the diffusion distance exists between the gas permeable PDMS channel boundaries and the flowing RBCs. In the current work, we have addressed hemocompatibility issues through the design of a microchannel network, modeled in many aspects after the pulmonary capillary system.[17,54] Such network models contain an open microchannel geometry with distributed posts to minimize hemolysis and thrombosis, while emphasizing a high surface-to-volume ratio for potential gas exchange. Similarly, we have fabricated a geometrically interconnected system of channels, whose structure allows us to specifically maintain low channel height while maximizing flow rate. Our goal in this study was to demonstrate, through simulation and experimentation, the flow dynamics and hemocompatibility of such a system. Our results demonstrate the following: 1) simulations indicate that at a flow rate of 0.250 ml/min, a moderate pressure drop can be achieved with a minimal hemolysis rate; and 2) hemocompatibility assays, obtained during perfusions of 6 and 12 hours at a flow rate predicted by the above simulations, demonstrated no significant hemolysis or microscopically visible thrombogenesis.

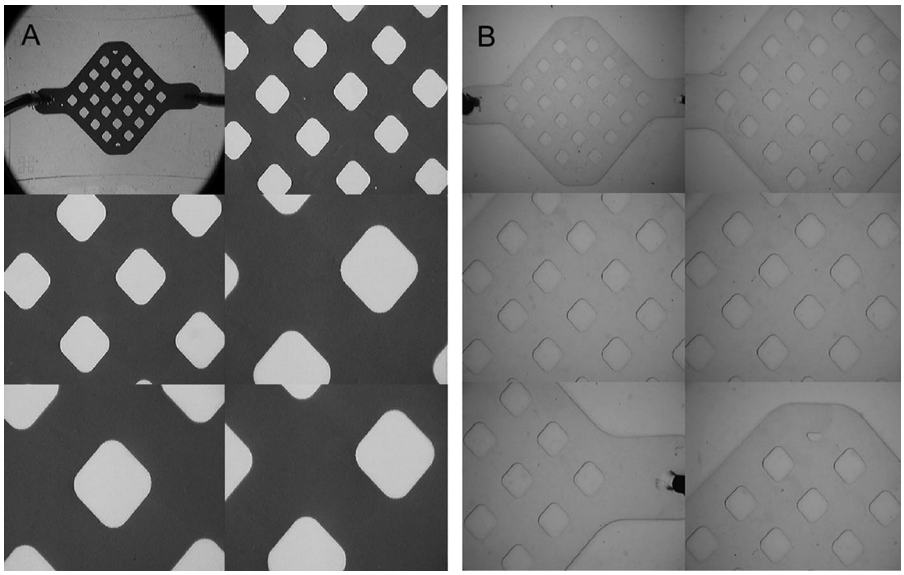

Figure 6. Determination of microscopic thrombus formation in the microfluidic device following 6-hour perfusion. The possibility of thrombus formation was studied by microscopy after a 6-hour perfusion at a constant flow rate of 0.250 ml/min. Images are displayed of various locations in the microchip at approximate magnifications ranging from 5× to 10×. Images are displayed immediately after the perfusion period (**left**) and after a flush with saline followed by ethanol/saline to detect residual microscopic thrombus formation (**right**). No thrombus was observed at any point of the device. For size reference, the width of single channels in the center of the device 1.197 mm while the inlet/outlet width is 3.38 mm.

Despite the advantages of short diffusion distance and laminar conditions at the microfluidic scale, the possibility of hemolysis due to high shear stress remains a critical limitation. Potential contributions to shear stress include not only geometrical factors, such as channel aspect ratio and sharp corners, but also the choice of device material itself in the fabrication of microfluidic conduits. Silicone rubbers, while used as medical device components and as instrumentation coatings, have the potential to exhibit some degree of thrombogenicity.[55,56] Of the silicone rubbers, PDMS is one of the most biocompatible, with low cytotoxicity and platelet activation in comparison to other siloxane blends.[55] PDMS is easy to mold and has superior optical clarity. However, its inherently hydrophobic surface makes it susceptible to nonspecific protein adhesion. While serum proteins in contact with PDMS microconduits act as potential blocking agents, the potential for more serious biofouling with long-term blood flow exists. Several approaches to surface modification exist to address this problem.[57–59] Both chemical and physical modifications of the PDMS surface can increase its biocompatibility by rendering the surface hydrophilic or entropically unfavorable for protein adhesion. These procedures include oxygen plasma treatment,[39] polymer coating or grafting,[60] and chemical treatment with strong acids.[1]

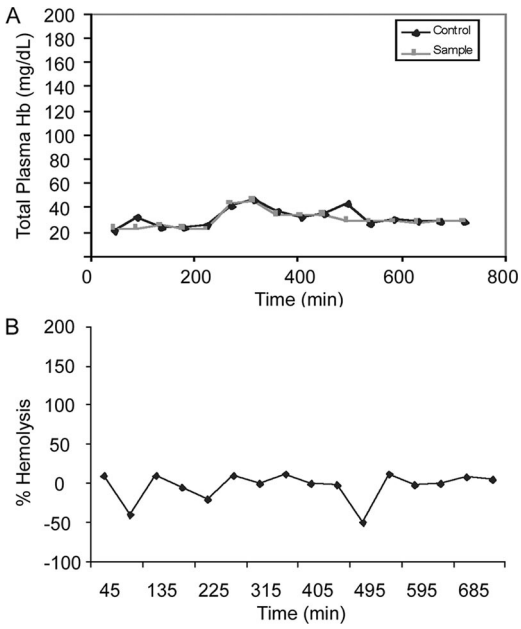

Figure 7. Assessment of hemocompatibility after 12-hour perfusion. (**A**) Hemolysis displayed as TPH as a function of flow through the microfluidic construct (sample) compared with flow outside of the microfluidic construct (control). Samples were obtained every 40 minutes over course of a 12-hour blood perfusion at a constant flow rate of 250 μl/min and TPH was assayed by spectrophotometry. (**B**) Hemolysis percentage represented as the [TPH (sample − control)/TPH (control)] during the course of the 12-hour blood infusion.

The RBC membrane consists of a lipid bilayer supported by a structural spectrin network.[61] Potential conditions under which membrane failure may occur include local and global strain and impaired spectrin formation, the formation of nonresealing pores, constitution of tethering effects, and actual membrane disruption.[62] The exposure of RBCs to low stress for short periods results in elastic deformation, which is reversible with removal of the stress (viscoelastic solid behavior). The same stress applied for longer periods results in a nonreversible shape change. Moreover, under conditions of high shear stress, the membrane yields and begins to flow resulting in a large degree of permanent deformation.[63] In this manner, it is evident that shear stress contributes to red cell damage, and importantly, may induce membrane effects which precede end-stage structural changes, or hemolysis. In the current study, we considered this important variable from the perspective of pressure drop across the device, and the simulated and direct assessments of hemolysis rate. Similar low rates of hemolysis were observed in recent demonstrations of PDMS-derived microfluidic devices employing low angle bifurcating channel configurations to separate plasma from whole blood.[64,65] One may predict that the simple minimization of shear stress in a system in which channel walls are cell-free

will result in a reduction of the probability that hemolysis will occur. However, a system more closely emulating a physiologic capillary which incorporates adherent endothelial cells would require a more comprehensive approach to the optimization of shear stress in the system, because the complex set of biologic response exhibited by the cells themselves must be considered.[66] Such design questions are beyond the scope of the present work, but will be considered in future iterations.

The underlying biologic, physical, and chemical processes underlying thrombogenesis in both native and artificial capillary systems have been extensively studied over the past several decades. This literature has emphasized the early biologic events underlying platelet activation,[67,68] as well as the complex interactions involving circulating platelets and endothelial surfaces,[69] intravascular fluid dynamics and transport,[49,70] and variations in capillary geometry.[71] The latter concept has particular relevance to the current work in that the capillary walls of our microfabricated system do not possess bioresponsive endothelial cells, and thus the critical determinants of platelet activation are variations in flow patterns induced by individual capillary structure and capillary network configuration. As previously hypothesized in the setting of model vascular stenosis,[72] platelet activation and surface attachment should be enhanced in regions of nonuniform flow possessing reduced flow velocity and patterns of recirculation. Such behavior may be associated with a greater propensity for flow streamlines perpendicular to the capillary wall and the resulting increase of convective platelet transport and platelet attachment.[73] In this context, several aspects of our system may be beneficial in reducing the likelihood of platelet aggregation and potential thrombus formation. Flow velocity simulation displays a high degree of uniformity as a function of location in the chip, in particular, in relation to posts, bifurcations, and level of channel intersections. Additionally, the microscopic demonstration of a lack of thrombus formation at 6 and 12 hours, although limited in capacity to detect early events associated with platelet activation and thus preliminary in nature, should thus be regarded as significant.

It is useful to consider to what extent the current microfluidic chip design in fact emulates the structure and function of the local pulmonary microcirculation, a network of geometrically interconnected and distensible capillary structures capable of transporting blood cells and of mediating physiologic gas exchange. The geometric properties exhibited by the pulmonary capillary network has been described in prior anatomical studies[74–77] and more recently by combined anatomical and physiologic simulations, based on realistic capillary number, length, diameter, and the degree of vessel interconnectedness.[17] Pulmonary blood flow is considered to be based on the presence of a complex array of short capillary segments, with apparent teleological benefits for regulating flow of red and white blood cells relative to lung expansion, phases of the cardiac cycle, and in response to local injury. Several properties of the naturally occurring network are present in the simplified network of microchannels presented in this report. For example, physiologic capillary networks are composed of arrays of functional segments of prescribed length (approximately 70 μm) and diameters (approximately 10 μm) and multiple three-way or four-way junctions.[38] Furthermore, there is considerable variability in the way in which capillary cross-sectional area and shape vary as a function of lung volume and transcapillary pressure.[17,78] This highly dynamic property of the pulmonary microcirculation is essential for maximizing gas exchange efficiency, while minimizing pressure drops and the resulting physical damage to flowing cells. Our artificial system emulated the interconnectedness of the naturally occurring capillary network, the functional length of the microcapillaries, and the relatively short diffusion distance. It should be noted that although PDMS has inherent mechanical elasticity,[79,80] fabrication of thin-wall devices emulating the dynamic of the biologic responsiveness of the pulmonary capillary remains a manufacturing challenge. Consequently, it was necessary to scale up the dimensions of the height and width of the microchannels (to ~0.1 and 1.1 mm, respectively) to allow uniform, laminar flow conditions and thus minimize damage to flowing cells. Our computational and experimental results confirm that the fabrication of a network of asymmetric PDMS-comprised microcapillaries is able to sustain uniform flow while maintaining hemocompatible conditions.

In summary, we have simulated and experimentally validated a microfluidic blood flow device, modeled generally after the pulmonary microcirculation and characterized by channels with a relatively high aspect ratio to maximize diffusivity and hemocompatibility and a network-type channel configuration to eliminate local flow irregularities. We predict that such as device will be applicable for artificial respiratory devices or in any instance where high rates of chemical diffusion must be balanced with biocompatibility.

Acknowledgments

This work was supported in part through grants from the Singapore-MIT alliance (SMA) and Progetto Roberto Rocca.

References

1. Fu AY, Spence C, Scherer A, *et al*: A microfabricated fluorescence-activated cell sorter. *Nat Biotechnol* 17: 1109–11, 1999.
2. McDonald JC, Duffy DC, Anderson JR, *et al*: Fabrication of microfluidic systems in poly (dimethylsiloxane). *Electrophoresis* 21: 27–40, 2000.
3. Srinivasan V, Vamsee KP, Fair RB: An integrated digital microfluidic lab-on-a-chip for clinical diagnostics on human physiological fluids. *Lab Chip* 4: 310–315, 2004.
4. Pei J, Tian F, Thundat T: Glucose biosensor based on the microcantilever. *Anal Chem* 76: 292–297, 2004.
5. Dittrich PS, Manz A: Lab-on-a-chip: Microfluidics in drug discovery. *Nat Rev Drug Discovery* 5: 210–218, 2006.
6. Khademhosseini A, Langer R, Borenstein J, Vacanti JP: Microscale technologies for tissue engineering and biology. *Proc Natl Acad Sci U S A* 103: 2480–24807, 2006.
7. Andersson H, van den Berg A: Microfabrication and microfluidics for tissue engineering: state of the art and future opportunities. *Lab Chip* 4: 98–103, 2004.
8. Narita Y, Hata K, Kagami H, *et al*: Novel pulse duplicating bioreactor system for tissue-engineered vascular construct. *Tissue Eng* 10: 1224–1233, 2004.
9. Mahoney MJ, Chen RR, Tan J, Saltzman WM: The influence of microchannels on neurite growth and architecture. *Biomaterials* 26: 771–778, 2005.
10. Emerson DR, Cieslicki K, Gu X, Barber RW: Biomimetic design of microfluidic manifolds based on a generalised Murray's law. *Lab Chip* 6: 447–454, 2006.

11. Irimia D, Toner M: Cell handling using microstructured membranes. *Lab Chip* 6: 345–352, 2006.
12. Park J, Berthiaume F, Toner M, *et al*: Microfabricated grooved substrates as platforms for bioartificial liver reactors. *Biotechnol Bioeng* 90: 632–644, 2005.
13. Mortensen JD: Intravascular oxygenator: a new alternative method for augmenting blood gas transfer in patients with acute respiratory failure. *Artif Organs* 16: 75–82, 1992.
14. Federspiel WJ, Hewitt TJ, Hattler BG: Experimental evaluation of a model for oxygen exchange in a pulsating intravascular artificial lung. *Ann Biomed Eng* 28: 160–167, 2000.
15. Dasse KA, Monzyk BF, Burckle E, *et al*: Development of a photolytic artificial lung: Preliminary concept validation. *ASAIO J* 49: 556–563, 2003.
16. Monzyk BF, Burckle E, Busch J, *et al*: Photolytic activation of a transition metal oxide thin film results in the generation of dissolved oxygen and increased oxyhemoglobin in whole blood. *ASAIO J* 52: 456–466, 2006.
17. Vollmer AP, Probstein RF, Gilbert R, Thorsen T: Development of an integrated microfluidic platform for dynamic oxygen sensing and delivery in a flowing medium. *Lab Chip* 5: 1059–1066, 2005.
18. Vollmer A: Development of an integrated microfluidic platform for oxygen sensing and delivery [master's thesis], Massachusetts Institute of Technology: Cambridge, MA, 2005.
19. Shevkoplyas SS, Gifford SC, Yoshida T, Bitensky MW: Prototype of an in vitro model of the microcirculation. *Microvasc Res* 65: 132–136, 2003.
20. Gifford SC, Frank MG, Derganc J, *et al*: Parallel microchannel-based measurements of individual erythrocyte areas and volumes. *Biophys J* 84: 623–633, 2003.
21. Trebotich D, Change W, Liepmann D: Modeling of blood flow in simple microchannels. *Proc Mod Simul Microsys*, 218–222, 2001.
22. Huang W, Yen RT, McLaurine M, Bledsoe G: Morphometry of the human pulmonary vasculature. *J Appl Physiol* 81: 2123–2133, 1996.
23. Gan RZ, Tian Y, Yen RT, Kassab GS: Morphometry of the dog pulmonary venous tree. *J Appl Physiol* 75: 432–440, 1993.
24. Kuhnle GE, Groh J, Leipfinger FH, *et al*: Quantitative analysis of network architecture, and microhemodynamics in arteriolar vessel trees of the ventilated rabbit lung. *Int J Microcirc Clin Exp* 12: 313–324, 1993.
25. Onuki T, Nitta S: Computer simulation of geometry and hemodynamics of canine pulmonary arteries. *Ann Biomed Eng* 21: 107–115, 1993.
26. Vollmer A, Snyder T, Kameneva M, *et al*: Development of a 2D microfluidic oxygenation device. Presented at the 51st Annual Meeting of the American Society for Artificial Internal Organs, Washington, DC, June 2005.
27. Huang Y, Doerschuk CM, Kamm RD: Computational modeling of RBC and neutrophil transit through the pulmonary capillaries. *J Appl Physiol* 90: 545–564, 2001.
28. Shin M, Matsuda K, Ishii O, *et al*: Endothelialized networks with a vascular geometry in microfabricated poly(dimethyl siloxane). *Biomed Microdev* 6: 269–278, 2004.
29. Kaazempur-Mofrad M, Vacanti JP, Krebs NJ, Borenstein JT: A MEMS-based renal replacement system, in *Proceedings of the solid state sensor, actuator, and microsystems workshop,* Hilton Head, SC, June 6–10, 2004.
30. Kaazempur-Mofrad M, Vacanti JP, Kamm RD: Computational modeling of flood flow and rheology in fractal microvascular networks in K.J. Bathe (ed), *Computational fluid and solid mechanics*, Oxford, Elsevier Science, Ltd. 2001, pp. 864–867.
31. Ballyk PD, Steinman DA, Ethier CR: Simulation of non-Newtonian blood flow in an end-to-side anastomosis. *Biorheology* 31: 565–586, 1994.
32. Fortin M, Esselaoui D: A finite element procedure for viscoelastic flows. *Int J Num Meth Fluids* 7: 1035–1052, 1987.
33. Eloot S, De Wachter D, Van Tricht I, Verdonck P: Computational flow modeling in hollow-fiber dialyzers. *Artif Organs* 26: 590–599, 2002.
34. Kuypers RA: Red cell membrane damage. *J Heart Valve Dis* 7: 387–395, 1998.
35. Blackshear PL, Dorman FD, Steinbach JH: Some mechanical effects that influence hemolysis. *ASAIO Trans* 11: 112–117, 1965.
36. Giersiepen M, Wurzinger LJ, Opitz R, Reul H: Estimation of shear stress-related blood damage in heart valve prostheses: In vitro comparison of 25 aortic valves. *Int J Artif Organs* 13: 300–306, 1990.
37. Zimmer R, Steegers A, Paul R, *et al*: Velocities, shear stresses and blood damage potential of the leakage jets of the Medtronic Parallel bileaflet valve. *Int J Artif Organs* 23: 41–48, 2000.
38. Lim WL, Chew YT, Chew TC, Low HT: Pulsatile flow studies of a porcine bioprosthetic aortic valve in vitro: PIV measurements and shear-induced blood damage. *J Biomech* 34: 1417–1427, 2001.
39. Xia YN, Whitesides GM: Soft lithography. *Ann Rev Mat Sci* 28: 153–184, 1998.
40. Whitesides GM, Ostuni E, Takayama S, *et al*: Soft lithography in biology and biochemistry. *Annu Rev Biomed Eng* 3: 335–373, 2001.
41. Thorsen T, Maerkl SJ, Quake SR: Microfluidic large-scale integration. *Science* 298: 580–584, 2002.
42. Belanger MC, Marois Y: Hemocompatibility, biocompatibility, inflammatory and in vivo studies of primary reference materials low-density polyethylene and polydimethylsiloxane: A review. *J Biomed Mater Res* 58: 467–477, 2001.
43. Litwin SB, Mitra SK, Von Colditz R, *et al*: Use of activated clotting time for monitoring anticoagulation during cardiopulmonary bypass in infants and children with congenital heart disease. *Cardiovasc Dis* 8: 364–371, 1981.
44. Hirsh J, Warkentin TE, Shaughnessy SG, *et al*: Heparin and low-molecular weight heparin. Mechanisms of action, pharmacokinetics, dosing considerations, monitoring, efficacy, and safety. *Chest* 114: 489–510, 1998.
45. Ferguson JJ: Conventional anti-thrombotic approaches. *Am Heart J* 130: 651–657, 1995.
46. Hattersley PG: Activated coagulation time of whole blood. *Am Med Assoc* 196: 436–440, 1966.
47. Malinauskas R: Plasma hemoglobin measurement techniques for the in-vitro evaluation of blood damage caused by medical device. *Artif Organs* 21: 1255–1267, 1997.
48. Zhang J, Gellman B, Koert A, *et al*: Computational and experimental evaluation of the fluid dynamics and hemocompatibility of the CentriMag blood pump. *Artif Organs* 30: 168–177, 2006.
49. Sorensen EN, Burgreen GW, Wagner WR, Antaki AF: Computational simulation of platelet deposition and activation: I. Model development and properties. *Ann Biomed Eng* 27: 436–448, 1999.
50. Siess W: Molecular mechanisms of platelet activation: *Physiol Rev* 69: 58–178, 1989.
51. Kim D, Chesler NC, Beebe DJ: A method for dynamic system characterization using hydraulic series resistance. *Lab Chip* 6: 639–44, 2006.
52. Fahraeus R, Lindqvist T: The viscosity of the blood in narrow capillary tubes. *Am J Physiol* 96: 562–568, 1931.
53. Reinke W, Johnson PC, Gaehtgens P: Effect of shear rate variation on apparent viscosity of human blood in tubes of 29 to 94 um diameter. *Circ Res* 59: 124–132, 1986.
54. Dhadwal A, Wiggs B, Doerschuk CM, Kamm RD: Effects of anatomic variability on blood flow and pressure gradients in the pulmonary capillaries. *J Appl Physiol* 83: 1711–1720, 1997.
55. Kobolow T, Tomlinson TA, Pierce JA: Blood compatibility of methyl, methyl vinyl, methyl phenyl, and trifluoropropylmethylvinyl silicone rubber without silica fillers in the spiral-coiled membrane lung. *J Biomed Mater Res* 11: 471–481, 1977.
56. Weathersby PK, Kolobow T, Stool EW: Relative thrombogenicity of polydimethylsiloxane and silicone rubber constituents. *J Biomed Mater Res* 9: 561–568, 1975.
57. Ratner BD, Castner DG (eds): *Surface modification of polymeric biomaterials*, Plenum Press, 1997.
58. Fan YL: in Wise DL (ed), *Encyclopedic handbook of biomaterials*

and bioengineering, Hydrophilic Lubricity in Medical Applications, Marcel Dekker, 1995, pp. 1331–1345.
59. Angelova N, Hunkeler D: Rationalizing the design of polymeric biomaterials. *TIBTech* 19: 409–421, 1999.
60. Hu S, Ren X, Bachman M, *et al*: Surface modification of poly(dimethylsiloxane) microfluidic devices by ultraviolet polymer grafting. *Anal Chem* 74: 4117–4123, 2002.
61. Mohandas M, Chasis JA, Shohet SB: The influence of membrane skeleton on red cell deformability, membrane material properties, and shape. *Semin Hematol* 20: 225–242, 1983.
62. Sallam AM, Hwang NH: Human red blood cell hemolysis in a turbulent shear flow: Contribution of Reynolds shear stresses. *Biorheology* 21: 783–797, 1984.
63. Hansen JC, Skalak R, Chien S, Hoger A: An elastic network model based on the structure of the red blood cell membrane skeleton. *Biophys J* 70: 146–166, 1996.
64. VanDelinder V, Groisman A: Separation of plasma from whole human blood in a continuous cross-flow in a molded microfluidic device. *Anal Chem* 78: 3765–3771, 2006.
65. Yang S, Undar A, Zahn JD: A microfluidic device for continuous, real-time blood plasma separation. *Lab Chip* 6: 871–880, 2006.
66. Tarbell JM, Weinbaum S, Kamm RD: Cellular fluid mechanics and mechanotransduction. *Ann Biomed Eng* 33: 1719–1723, 2005.
67. Offermanns S: Activation of platelet function through G protein-coupled receptors. *Circ Res* 99: 1293–1304, 2006.
68. Kahner BN, Shankar H, Murugappan S, *et al*: Nucleotide receptor signaling in platelets. *J Thromb Haemost* 4: 2317–2326, 2006.
69. Karpman D, Manea M, Vaziri-Sani F, *et al*: Platelet activation in hemolytic uremic syndrome. *Semin Thromb Hemost* 32: 128–145, 2006.
70. Basmadjian D: The effect of flow and mass transport in thrombogenesis. *Ann Biomed Eng* 18: 685–709, 1990.
71. Schoephoerster RT, Oynes F, Nunez G, *et al*: Effects of local geometry and fluid dynamics on regional platelet deposition on artificial surfaces. *Arterioscler Throm* 13: 1806–1813, 1993.
72. Schmid-Schoenbein H, Born GVR, Richardson PD, *et al*: Rheology of thrombotic processes in flow: The interaction of erythrocytes and thrombocytes subjected to high flow forces. *Biorheology* 18: 415–444, 1981.
73. Karino T, Goldsmith HL: Adhesion of human platelets to collagen on the walls distal to a tubular expansion. *Microvasc Res* 17: 238–262, 1979.
74. Staub N, Schultz E: Pulmonary capillary length in dog, cat and rabbit. *Resp Physiol* 5: 371–378, 1968.
75. Poppel AS: Network models of peripheral circulation, in Skalak R, Chien S (eds), *Handbook of bioengineering*. New York, McGraw Hill, 1987, 20.1–20.24.
76. Pries AR, Secomb TW, Gaehtgens P, Gross JF: Blood flow in microvascular networks: Experiments and simulation. *Circ Res* 67: 826–834, 1990.
77. Secomb TW: Mechanics of blood flow in microcirculation, in Ellington CP, Pedley TJ (eds), *Biological fluid dynamics*, Cambridge, UK, Company of Biologists, 1995, pp. 305–321.
78. Fung YC, Sobin SS: Pulmonary alveolar blood flow. *Circ Res* 30: 470–490, 1972.
79. Martin DJ, Warren LA, Gunatillake PA, *et al*: Polydimethylsiloxane/polyether-mixed macrodiol-based polyurethane elastomers: Biostability. *Biomaterials* 21: 1021–1029, 2000.
80. Mata A, Fleischman AJ, Roy S: Characterization of polydimethylsiloxane (PDMS) properties for biomedical micro/nanosystems. *Biomed Microdev* 7: 281–293, 2005.